



Raman spectra and structural stability in B-site manganese doped $(\text{Bi}_{0.5}\text{Na}_{0.5})_{0.925}\text{Ba}_{0.075}\text{TiO}_3$ relaxor ferroelectric ceramics

J. Anthoniappen^{a,g,*}, C.S. Tu^b, P.-Y. Chen^c, C.-S. Chen^d, Y.U. Idzerda^e, S.-J. Chiu^f

^a Graduate Institute of Applied Science and Engineering, Fu Jen Catholic University, New Taipei City 24205, Taiwan

^b Department of Physics, Fu Jen Catholic University, New Taipei City 24205, Taiwan

^c Department of Mechanical Engineering, Ming Chi University of Technology, New Taipei City 24301, Taiwan

^d Department of Mechanical Engineering, Hwa Hsia University of Technology, New Taipei City 23567, Taiwan

^e Department of Physics, Montana State University, Bozeman, MT 59717, USA

^f National Synchrotron Radiation Research Center, Hsinchu 30076, Taiwan

^g Department of Physics, University of San Carlos, Cebu City 6000, Philippines

Received 21 March 2015; received in revised form 1 May 2015; accepted 2 May 2015

Available online 21 May 2015

Abstract

Soft X-ray absorption (XAS), transmission electron spectroscopy (TEM), Raman spectroscopy, and synchrotron XRD have been studied in B-site 0–2 mol% manganese (Mn) doped $(\text{Bi}_{0.5}\text{Na}_{0.5})_{0.925}\text{Ba}_{0.075}\text{TiO}_3$ (BN7.5BT) relaxor ferroelectric ceramics. High-resolution synchrotron XRD and TEM reveal two phase coexistence of rhombohedral $R3c$ and tetragonal $P4bm$ structures in 0 and 0.2%, and an orthorhombic structure in 1 and 2% Mn-doped BN7.5BT at room temperature. Raman spectra of 0% Mn reveal structural transition from two phase coexistence to tetragonal phase near 190 °C with a softening anomaly, while 0.2–2% Mn-doped BN7.5BT show softening behavior near 290 °C upon heating. Raman spectra and synchrotron XRD indicate that Mn doping can enhance structural thermal stability in BN7.5BT ceramics.

© 2015 Elsevier Ltd. All rights reserved.

Keywords: Relaxor ferroelectric ceramics; Raman spectroscopy; Synchrotron XRD; Phase transition

1. Introduction

Lead-free bismuth sodium titanate $(\text{Bi}_{0.5}\text{Na}_{0.5})\text{TiO}_3$ (BNT) based materials have attracted so much attention because of their promising piezoelectric and electromechanical properties, which are comparable to lead based $\text{Pb}(\text{Zr},\text{Ti})\text{O}_3$ (PZT) piezoceramics [1]. Among the studied materials, solid solutions between a rhombohedral (BNT) and tetragonal BaTiO_3 (BT) (abbreviated as BN100xBT) have been of particular interest due to the existence of morphotropic phase boundary (MPB) between rhombohedral (R) and tetragonal (T) structures near

$x=0.06\text{--}0.08$ [2–5]. Though piezoelectric and dielectric properties in MPB compositions of BN100xBT are remarkably enhanced, the depolarization temperature T_d and Curie temperature T_c significantly were reduced at the MPB. In contrast to PZT the MPB in BN100xBT is strongly curved, thus leading to low-temperature stability [6]. For applications, the properties of BN100xBT ceramics need to be further improved. It has been reported that optimizing processing and modifying are major ways to improve piezoelectric properties [7].

Several studies have been reported on effects of manganese doping on lead based and lead-free solid solutions. It was found that Mn substitution could be effective in inducing hard characteristics in $(1-y)\text{Pb}(\text{Zn}_{1/3}\text{Nb}_{2/3})\text{O}_3-y\text{PbTiO}_3$ (PZNT) single crystals [8,9]. Luo et al. [10] showed increments of coercive field, Curie temperature, and stability of the ferroelectric rhombohedral phase in 3 at% Mn-doped $0.71\text{Pb}(\text{Mg}_{1/3}\text{Nb}_{2/3})\text{O}_3-0.29\text{PbTiO}_3$ (PMNT) single crystals.

* Corresponding author. Fu Jen Catholic University/SVD Residence, 510, Zhongzheng Road, Xinzhuang Dist, New Taipei City 24205, Taiwan. Tel.: +886 2901 4112; fax: +886 02 2903 3153.

E-mail address: jesusvd@gmail.com (J. Anthoniappen).

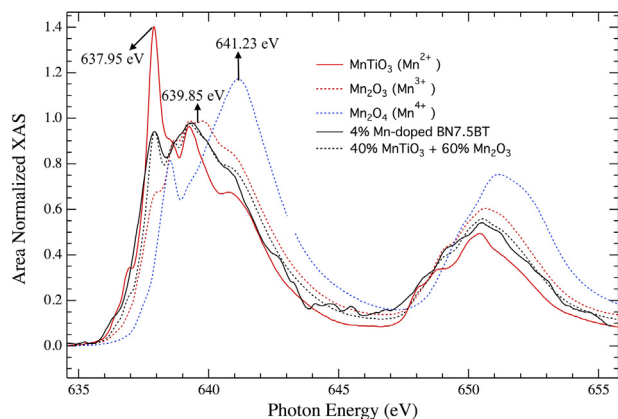


Fig. 1. Mn L-edge XAS signals in BN7.5BT-4% Mn sample at room temperature. The solid black line is the experimental data. Red, blue and pink lines are a set of standards for various Mn valences. The green dashed line is the sum of the Mn^{2+} and Mn^{3+} spectra. (For interpretation of the references to color in this figure legend, the reader is referred to the web version of this article.)

Yan et al. [11] proposed that Mn^{3+} substitution on Ti and Zr sites of $0.8Pb(Zr_{0.52}Ti_{0.48})O_3-0.2Pb(Zn_{1/3}Nb_{2/3})O_3$ (PZT-PZN) ceramics induces hardening effect, whereas Mn^{2+} substitution on the Zn-site stabilizes the perovskite phase. Priya et al. [12] conducted Mn-doping on the PZT modified by 20 mol% $Pb(Zn_{1/3}Nb_{2/3})O_3$ (PZN) relaxor material, and their studies indicated low dielectric loss and high mechanical quality factor Q_m . In manganese oxide doped hard PZT compositions, domain wall motion could be pinned by the oxygen vacancy resulting in reduction of dielectric loss as well as enhancement of Q_m [12].

Zhang et al. [13] reported that Mn doping in BN100xBT single crystal could enhance ferroelectric and piezoelectric properties significantly. The piezoelectric constant d_{33} and electromechanical coupling coefficients (k_t and k_{31}) were found to be 483 pC/N, 0.56, and 0.40, respectively. Sapper et al. [14] discovered that Mn-doped BN100xBT piezoceramics stabilize macroscopic polarization and consequently shift depolarization temperature (T_d) to higher temperatures as compared to the undoped BN100xBT. It was found that the suitable substitution of Mn ion into the B site induces the lattice distortion of perovskite MnO-doped $(Na_{0.5}Bi_{0.5})_{0.92}Ba_{0.08}TiO_3$ lead-free piezoceramics [15]. Temperature-dependent dielectric permittivity indicates that the MnO addition reconstructs the disorder array destroyed by joining $BaTiO_3$ in the $Bi_{0.5}Na_{0.5}TiO_3$ system due to the sizable radius of the B-site cations [15].

Yao et al. [16] studied domain structure, octahedral tilting, and lattice structure of Mn:NBT-5.5%BT single crystals using bright field and lattice imaging, and selected area electron diffraction (SAED). They reported the following results with Mn substitution: (i) increased tendencies of FE ordering and in-plane octahedral tilting; (ii) formation of structural modulation across domain boundaries, which may help relax elastic stress between FE domains; and (iii) an increase in the number of in-phase oxygen tilted regions, with a size of about 2–8 nm and with a tendency of alignment along $\{110\}$. The Mn-doped NBT-6%BT single crystals have

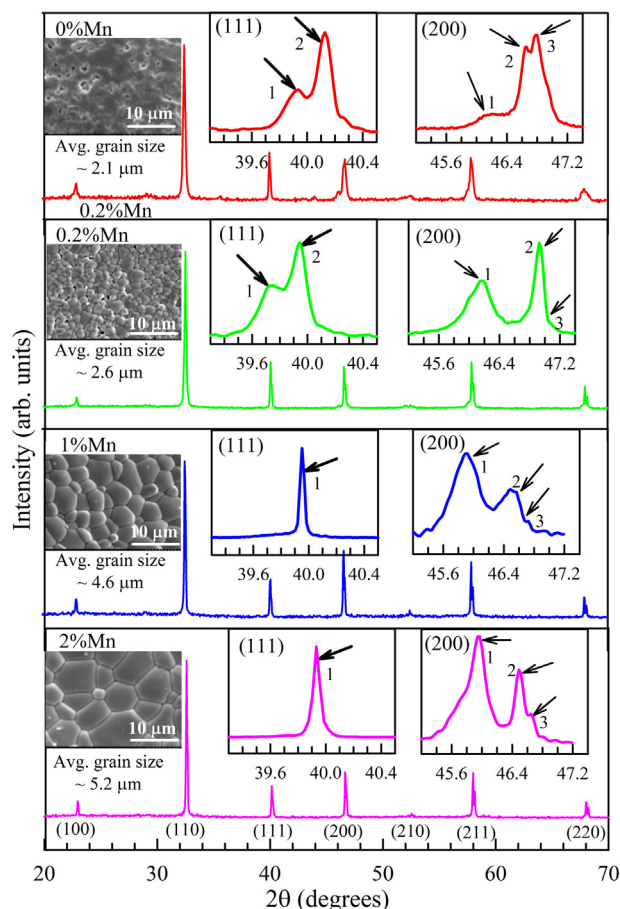


Fig. 2. Synchrotron XRD spectra in the range of $20-70^\circ$ at room temperature. The insets are corresponding (111) and (200) diffraction patterns and cross-section SEM micrographs.

shown that the tetragonal domain states could be stabilized by poling along $[001]$ direction and the piezoelectric coefficient d_{33} could reach 570 pC/N [17]. Recently we have reported that 0.5 mol% Mn doping in $(Bi_{0.5}Na_{0.5})_{1-x}Ba_xTiO_3$ ($x=0$ and 0.075) solid solutions can increase structural thermal stability, depolarization temperature (T_d), piezoelectric coefficient (d_{33}), and electromechanical coupling factor (k_t) [18].

Thermal phase stability is essential for applications. So far, there is very little understanding about the structural stability induced by Mn-doping in BNBT solid solutions. Raman spectroscopy has been used as an effective technique to investigate the structural evolution in perovskite-type solid solution ceramics [19,20]. In this work, we have studied the effects of MnO_2 doping in BN7.5BT $[(Bi_{0.5}Na_{0.5})_{0.925}Ba_{0.075}(Ti_{1-x}Mn_x)O_3]$ via micro-Raman spectroscopy and synchrotron X-ray diffraction (XRD) as functions of temperature for a sequence of Mn concentrations ($x=0-2\%$ Mn). Our results confirm that the MnO_2 doping can enhance structural phase thermal stability.

2. Experimental procedure

$(Bi_{0.5}Na_{0.5})TiO_3$ (BNT) and $(Bi_{0.5}Na_{0.5})_{0.925}Ba_{0.075}(Ti_{1-x}Mn_x)O_3$ (BN7.5BT- x Mn) ($x=0, 0.2, 1.0, \text{ and } 2.0$ mol%)

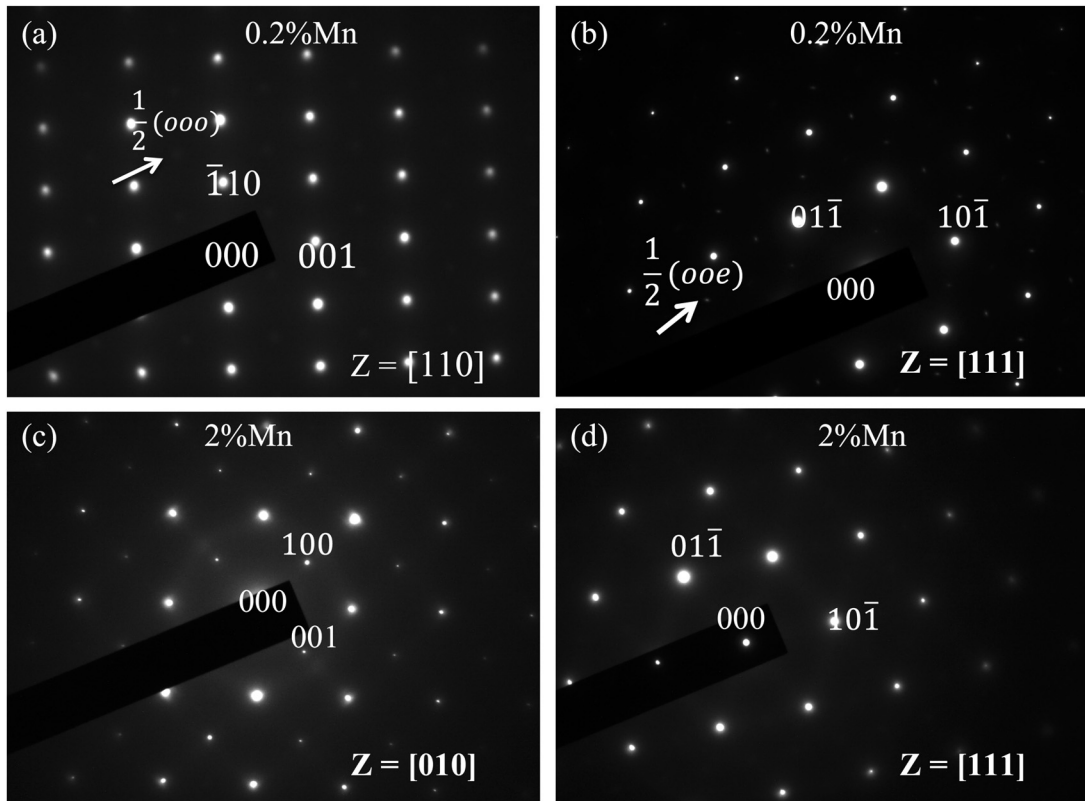


Fig. 3. Selected area diffraction patterns (SADP) of 0.2% Mn viewed along (a) [1 1 0] and (b) [1 1 1] zone axis. SADPs of 2% Mn viewed along (c) [0 1 0] and (d) [1 1 1] zone axis. Arrows labeled in the SADPs indicate superlattice reflections.

ceramics were prepared by using solid state reaction. High purity (>99%) powders of Bi₂O₃, Na₂CO₃, BaCO₃, TiO₂, and MnO₂ were used as starting materials. Stoichiometric amounts of powders were ball-milled for more than 24 h in ethanol. The mixture was calcined at 900 °C (2 h) and a Retsch PM100 planetary ball mill was used to reduce particle size. The calcined powders were then pressed into 1.0 cm-diameter disks for sintering at 1150 °C (2 h) and 1170 °C (2 h) for BNT and BN7.5BT-xMn, respectively. All polished sintered

samples were annealed at 600 °C for 30 min to remove residual stress.

Raman spectra were measured using a micro-Raman instrument (Nanobase, XperRam 200) equipped with a green laser of $\lambda = 532$ nm and a TE-cooled CCD detector (1024 × 128 pixel). A high magnification objective (40×, 0.75 NA) was used to focus the laser to a spot of ~1 μm. For temperature-dependent Raman scattering measurements, the data were taken upon heating from 25 °C to 290 °C. The high-resolution synchrotron XRD

Table 1
Raman vibration frequencies (ω) and their mode assignments of (Bi_{0.5}Na_{0.5})TiO₃ (BNT) and BaTiO₃ (BTO) ceramics.

Phonon mode assignment in polycrystalline Bi _{0.5} Na _{0.5} TiO ₃ at -110 °C			Phonon mode assignment in polycrystalline BaTiO ₃ at 25 °C		
Mode frequency ω (cm ⁻¹)	Mode assignment	References	Mode frequency ω (cm ⁻¹)	Mode assignment	References
130	A ₁ (1)	[24–26]	112	E(1)	[36]
164*	E(1)		181	E(2)	[33–36]
192*	E(2)		263	A ₁ (1)	[33,34]
244	E(3)	[27]	306	B ₁	[33,34,36]
287	A ₁ (2)	[25,26,28]	485	E(3)	[34,35]
335	A ₁ (3)	[27]	527	A ₁ (2)	[33,34,36]
412*	E(4)		531	E(4)	[35,38]
480	E(5)	[26,27,29]	716	A ₁ (3)	[33–35]
521	A ₁ (4)	[26,27,29]			
577	E(6)	[26,27,29]			
720	E(7)	[27]			
780	E(8)	[27]			
852	E(9)	[27]			

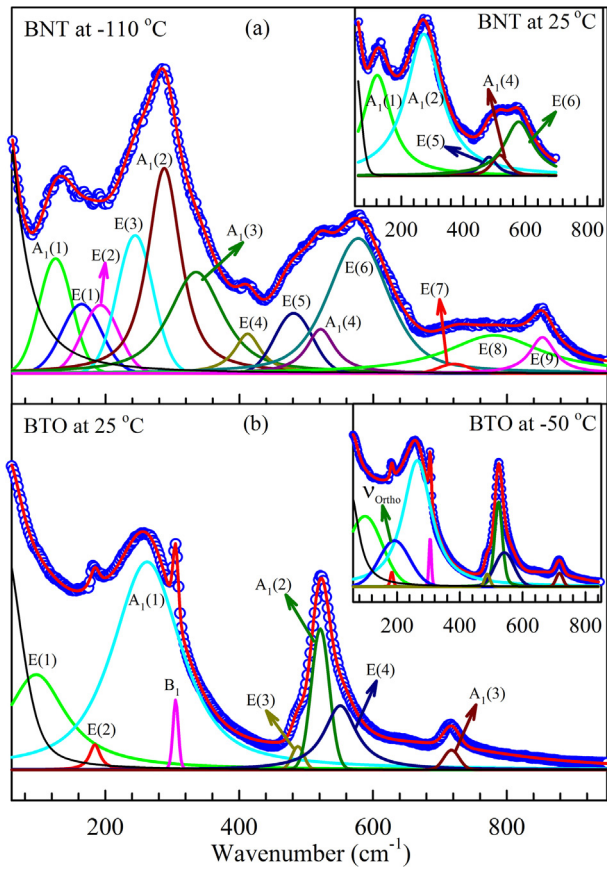


Fig. 4. (a) Raman spectra of rhombohedral $\text{Bi}_{1/2}\text{Na}_{1/2}\text{TiO}_3$ (BNT) at -110°C in the range of $60\text{--}950\text{ cm}^{-1}$. Corresponding inset is the spectra at room temperature with dominant modes. (b) Raman spectra of BaTiO_3 (BTO) at 25°C . Corresponding inset is the spectra in the orthorhombic phase (at -50°C) with dominant modes.

was performed at NSRRC (BL17B1) in Taiwan with a photon energy of 8 keV ($\lambda = 1.555\text{ \AA}$). Both Raman and XRD spectra were fitted by using PeakFit software with the sum of Gaussian and Lorentzian profiles. Grain morphologies were obtained using a scanning electron microscope (SEM; HITACHI S-3400N FE-SEM). High-resolution transmission electron microscopy (TEM) observations were carried out using the JEOL JEM-2100 LaB6. To determine oxidation states, the soft X-ray absorption spectra (XAS) of Mn $L_{2,3}$ -edge were recorded in total electron yield via sample current mode at beamline 6.3.1.1 of Advanced Light Source Berkeley National Laboratory. Absorption measurements were made at room temperature with linear photon polarization and normal incidence.

3. Results and discussion

Fig. 1 shows the normalized Mn L-edge X-ray absorption spectra (XAS) measured from 4% Mn-doped BN7.5BT ceramics. We believe that 4 mol% Mn is within the limit to represent our compositions studied in this work. The spectra have been normalized to the integrated peak area ($L_2 + L_3$) and energy is calibrated by comparing the peak position of Mn_3O_4 reference powder that is simultaneously collected with each sample spectra. The 2nd peak energy of the reference powder is set to

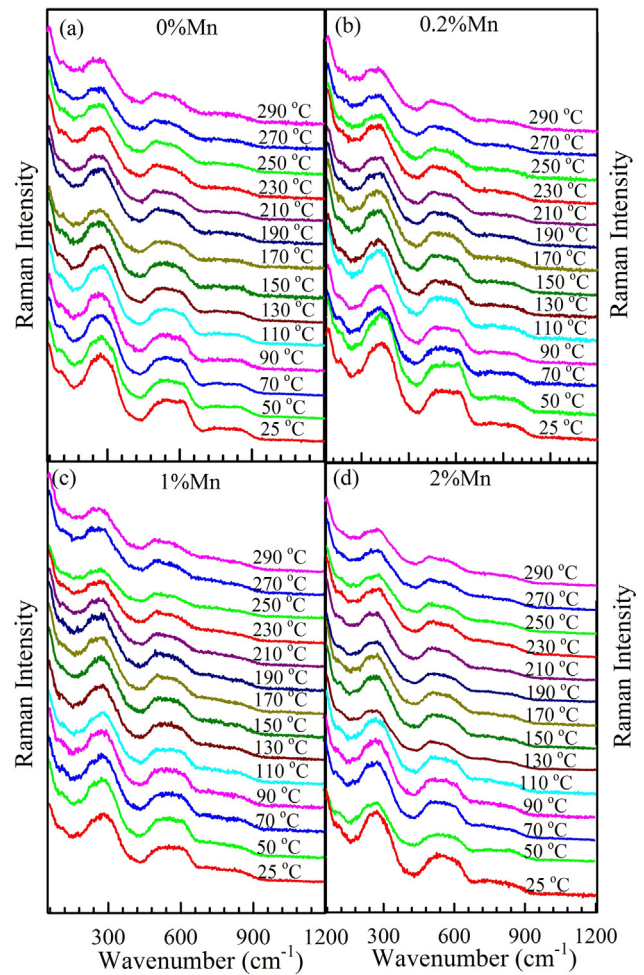


Fig. 5. Temperature evolution of Raman spectra of (a) 0% Mn, (b) 0.2% Mn, (c) 1% Mn, and (d) 2% Mn.

640.05 eV . All reference powder samples are normalized by the number of d-holes, resulting in absorption spectra per d-hole. The binding energy at the absorption edge for each standard Mn is indicated by arrow marks. The measured spectra can be well fit from a linear combination of two reference powder spectra ($\sim 40\%$ of the Mn^{2+} and $\sim 60\%$ of Mn^{3+}), to give an indication of the average Mn valence. This result indicates an effective equilibrium of divalent Mn^{2+} ($\sim 40\%$) and trivalent Mn^{3+} ($\sim 60\%$) in the sintered sample, although manganese presents as tetravalent Mn^{4+} in the dopant oxide MnO_2 . According to the Hume Rothery rule, the difference in ionic size between solute and solvent ions should be less than 15% to form a stable solid solution [11]. Ionic radius of Mn^{3+} (0.645 \AA) is similar to that of Ti^{4+} (0.605 \AA) and much smaller than Bi^{3+} (1.03 \AA) and Ba^{2+} (1.38 \AA) ions. Ionic radius of Mn^{2+} (0.83 \AA) is 22.5% larger than Ti^{4+} , but is 20% and 55% smaller than Bi^{3+} and Ba^{2+} ions, respectively. Therefore, it is likely that Mn^{3+} ions occupy B-site replacing Ti^{4+} causing oxygen vacancies, and Mn^{2+} ions may distribute at grain boundaries.

The density of the samples were measured by Archimedes method, and are respectively ~ 5.70 , 5.75 , 5.83 and 5.87 g/cm^3 for 0.0, 0.2, 1.0, and 2% Mn, which are above 96% of the theoretical density. Fig. 2 shows synchrotron XRD patterns taken at

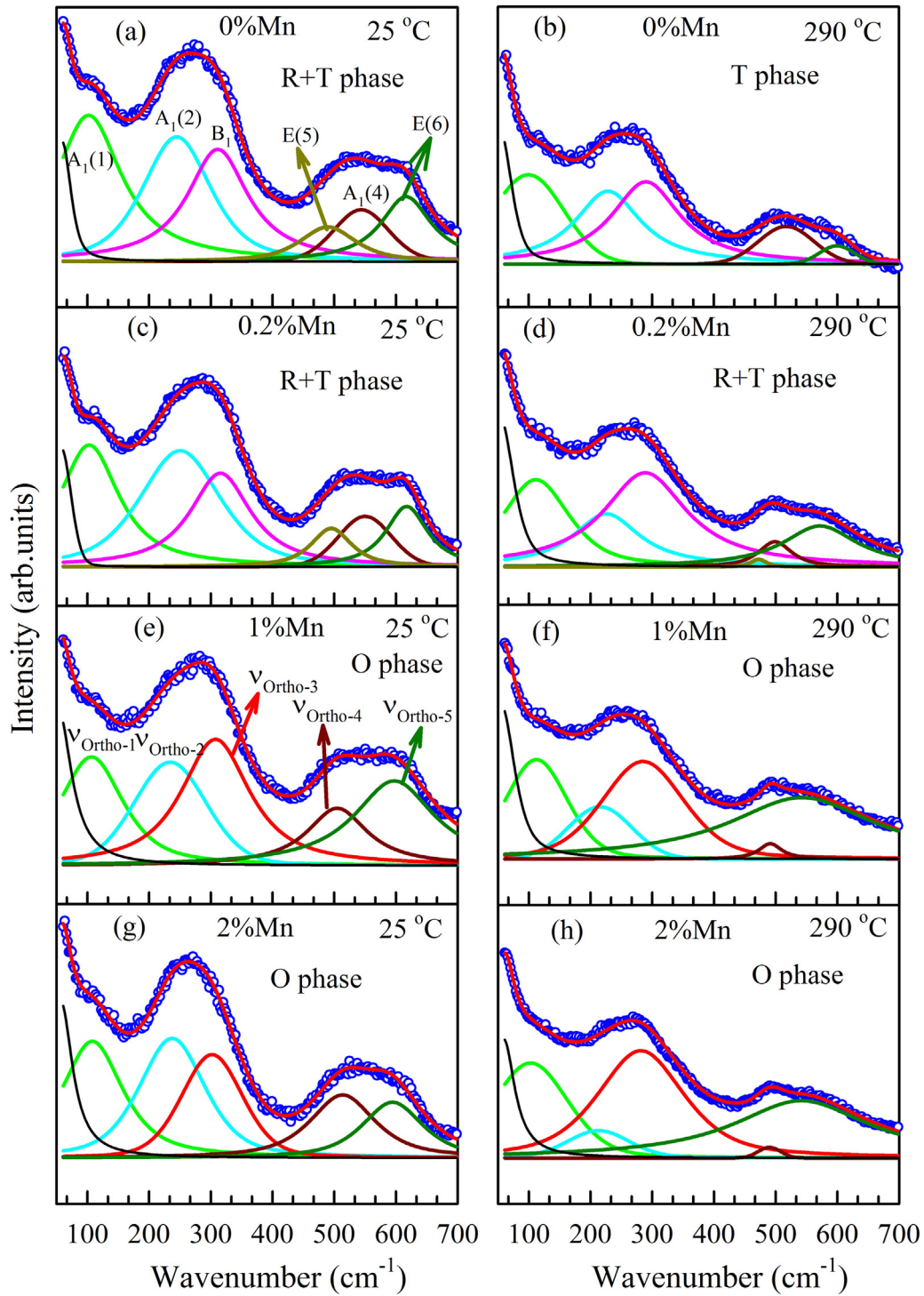


Fig. 6. Fits of Raman vibrational bands for 0% Mn, 0.2% Mn, 1% Mn, and 2% Mn at 25 °C and 290 °C. Dominant modes are labeled with arrow marks.

Table 2
Frequencies of dominant Raman modes at room temperature in 0–2% Mn-doped BN7.5BT ceramics.

Composition	A–O band (cm ⁻¹)	B–O band (cm ⁻¹)		BO ₆ octahedra (cm ⁻¹)	
0%Mn	102	258	310	525	615
0.2%Mn	103	250	308	520	611
1%Mn	103	237	307	513	597
2%Mn	104	232	305	505	594

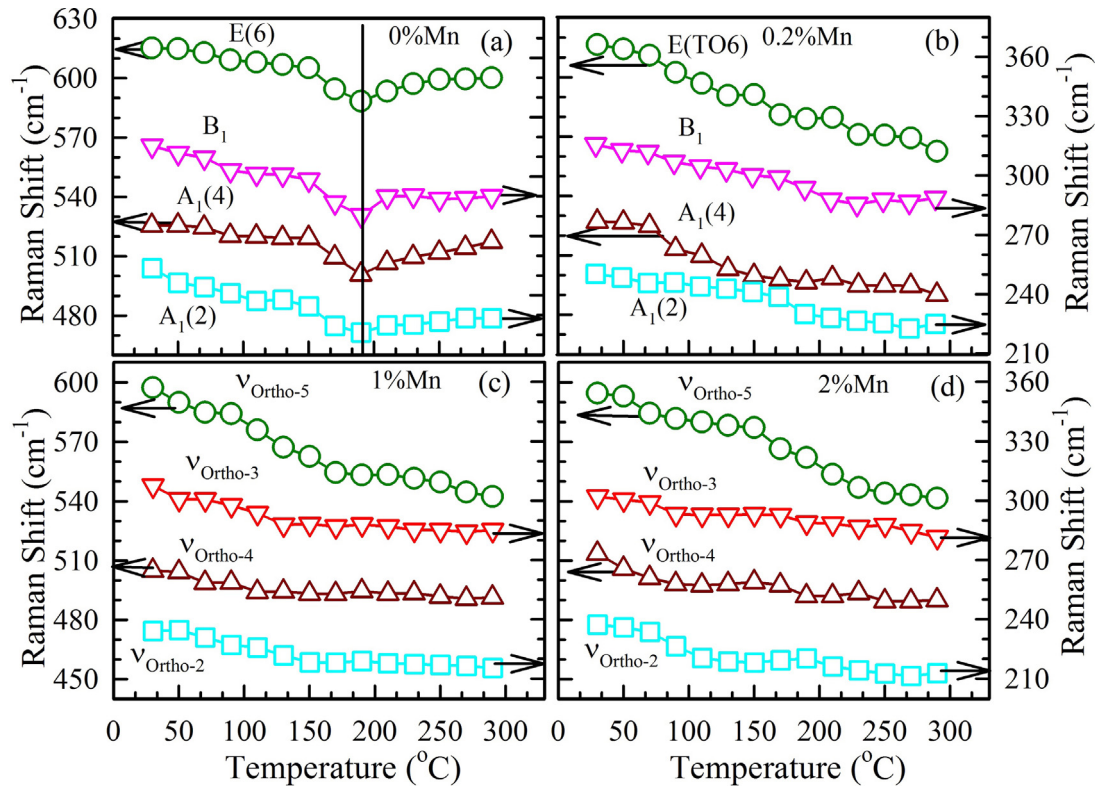


Fig. 7. Temperature evolution of dominant Raman modes.

room temperature. The insets (on the left side) show the SEM grain morphologies of the cross-section, obtained after thermal etching at 1000 °C for 3 min. The grain size increases with MnO₂ and the average grain sizes are 2.1, 2.6, 4.6, and 5.2 μm for 0, 0.2, 1.0, and 2% Mn, respectively. The insets are diffraction patterns of (1 1 1) and (2 0 0) reflections at room temperature with peaks marked with numbers and arrows. The 0 and 0.2% Mn show two phase coexistence (rhombohedral and tetragonal) evidenced by three (2 0 0) peaks and two (1 1 1) peaks. Whereas, 1 and 2% Mn show orthorhombic structure evidenced by three distinct (2 0 0) peaks and one sharp (1 1 1) peak.

As shown in Fig. 3, the as-identified structures are further confirmed by selected area diffraction patterns (SADP) from high-resolution TEM for 0.2 and 2% Mn. The phase coexistence in 0% Mn-doped BN7.5BT has been shown in our previous work [5]. Fig. 3(a) reveals the $1/2\{ooo\}$ superlattice diffraction spots along [1 1 0] zone axis, which belong to $R3c$ phase with single-axis anti-phase $a^-a^-a^-$ octahedral tilting. Fig. 3(b) shows the $1/2\{ooe\}$ superlattice diffraction spots along [1 1 1] zone axis, which is the characteristic of the tetragonal $P4bm$ symmetry with three-axis equivalent in-phase $a^o a^o c^+$ octahedral tilting. This confirms two phase coexistence ($R+T$) in 0.2% Mn. Fig. 3(c and d) do not show any superlattice diffraction pattern in 2% Mn, thus ruling out the possibilities of rhombohedral $R3c$ and tetragonal $P4bm$ symmetries. However, one can observe that the direction of both $\{100\}$ diffractions in $[010]$ -zoned SADP (Fig. 3c) is orthogonal to each other, and three sets of $\{110\}$ diffractions in the $[111]$ -zoned SADP (Fig. 3d) have different

distances from the transmission spots. These TEM results suggest an orthorhombic structure in 2% Mn-doped BN7.5BT at room temperature.

Before going into Raman spectra of Mn-doped BN100xBT compositions, the Raman spectra of both end compositions ($\text{Bi}_{0.5}\text{Na}_{0.5}\text{TiO}_3$ (BNT) and BaTiO_3 (BTO) were analyzed. BNT is a well-known classic rhombohedral ferroelectric material at ambient temperature and belongs to the space group $R3c$ (C_{3v}^6) [21,22], containing two formula units ($Z=2$) [23]. The group theory leads to $5A_1$, $5A_2$, and $10E$ vibrational modes for rhombohedral BNT. One A_1 and one doubly degenerate E mode correspond to acoustic phonons, and $5A_2$ modes are Raman silent modes. Therefore, the irreducible representation of 13 Raman and IR active modes is $\Gamma_{\text{BNT}} = 4A_1 + 9E$ [24]. BNT shows a tetragonal $P4bm$ (C_{4v}^2) structure (formula units, $Z=2$) at 698 K, determined by neutron powder diffraction [25]. Based on the nuclear site group analysis, the main Raman active modes in the space group $P4bm$ structure ($Z=2$) include A_1 , B_1 , B_2 , and E modes [19].

Fig. 4(a) shows the deconvoluted spectrum of BNT at -110°C with 13 Raman modes in the range of $60\text{--}950\text{ cm}^{-1}$. The samples were cooled down from room temperature to -150°C and then the spectra were obtained from -110°C by steps upon heating. The inset shows the spectrum of dominant modes at 25°C , which is similar to that measured at -110°C , except that the Raman bands at -110°C are relatively sharper due to less phonon interaction. A compilation of Raman vibration frequencies and their modes in rhombohedral ($R3c$) BNT are

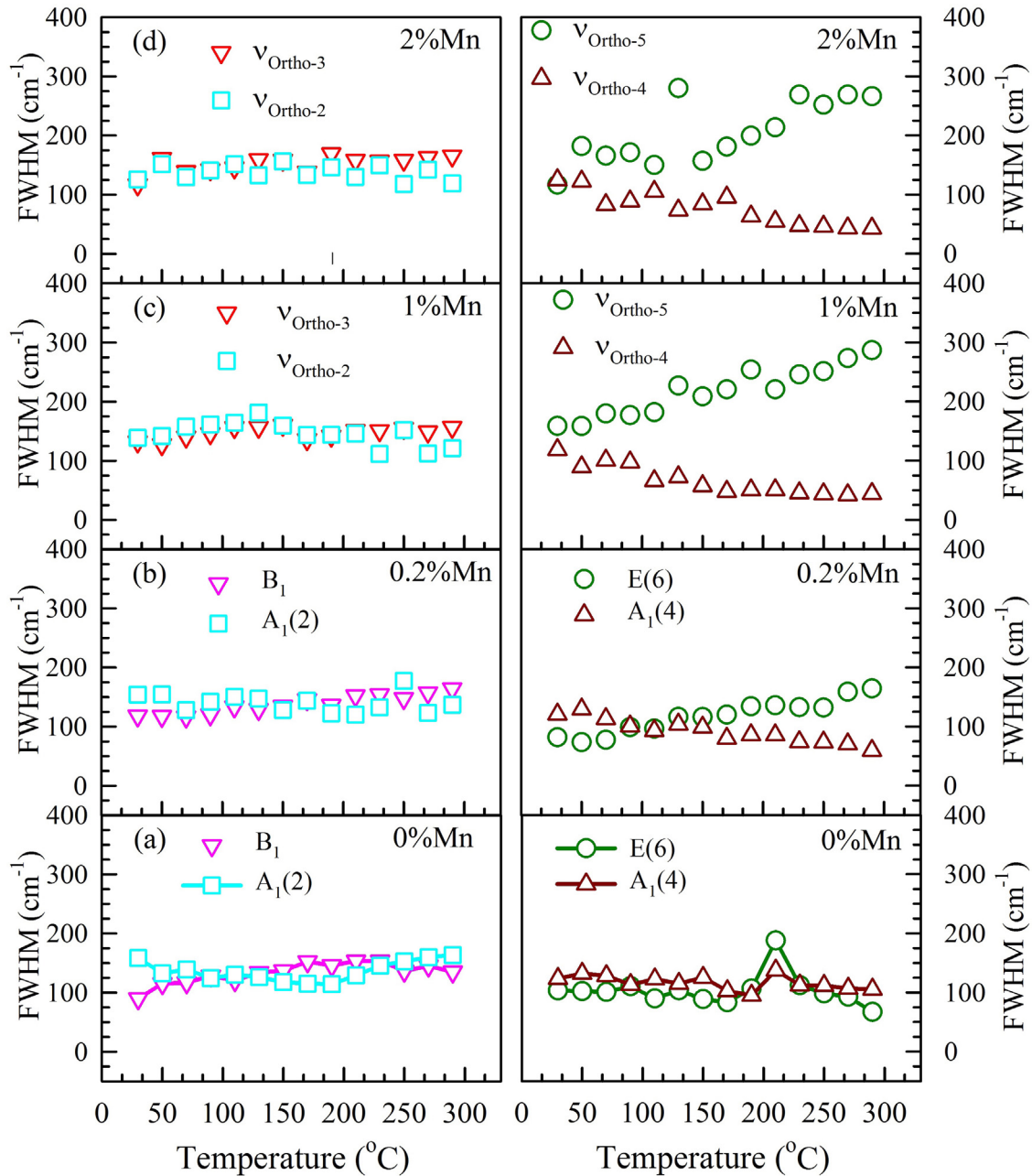


Fig. 8. Variation of full width at half maxima (FWHM) of dominant Raman modes.

given in Table 1. In addition to Raman modes found in previous works [24,26–30], Raman vibrations of 164, 192, and 412 cm^{-1} have been identified as labeled by “*”. Bands located in the range of 100–200 cm^{-1} are assigned to Na/Bi–O stretching vibrations. Bands located in the range of 200–600 cm^{-1} are mainly associated with Ti–O stretching vibrations. In particular, the 287 cm^{-1} mode involves only O–Ti–O bending motion, which is sensitive to the phase transition [26]. High-frequency Raman bands are dominated by vibrations involving oxygen displacements [31]. The high frequency modes (600–850 cm^{-1}) have been assigned to vibrations of the TiO_6 oxygen octahedral [24].

Fig. 4(b) shows the deconvoluted phonon spectra of BTO at 25 °C. BTO exhibits four different phases upon heating:

a rhombohedral $R3m$ phase below -90°C , an orthorhombic $Amm2$ phase at -90 to 6°C , a tetragonal $P4mm$ phase at 6 to 130°C , and a cubic phase $Pm\bar{3}m$ above 130°C [32,33]. The Raman active modes in the tetragonal $P4mm$ space group ($Z=1$) can be represented by the irreducible representation; $\Gamma_{\text{Raman, BTO}} = 3A_1 + B_1 + 4E$ [32]. The B_1 mode indicates asymmetric motion of the TiO_6 octahedral and the $A_1(3)$ is related to the highest-wavenumber longitudinal optical mode [34]. Note that major Raman modes of BNT in the space group $P4bm$ structure ($Z=2$) also have A_1 , B_1 , and E modes [25]. Based on the previous studies [35,36], the Raman spectra of orthorhombic and tetragonal phases in BTO are similar. The only difference is the appearance of ν_{ortho} vibration at 192 cm^{-1} in orthorhombic

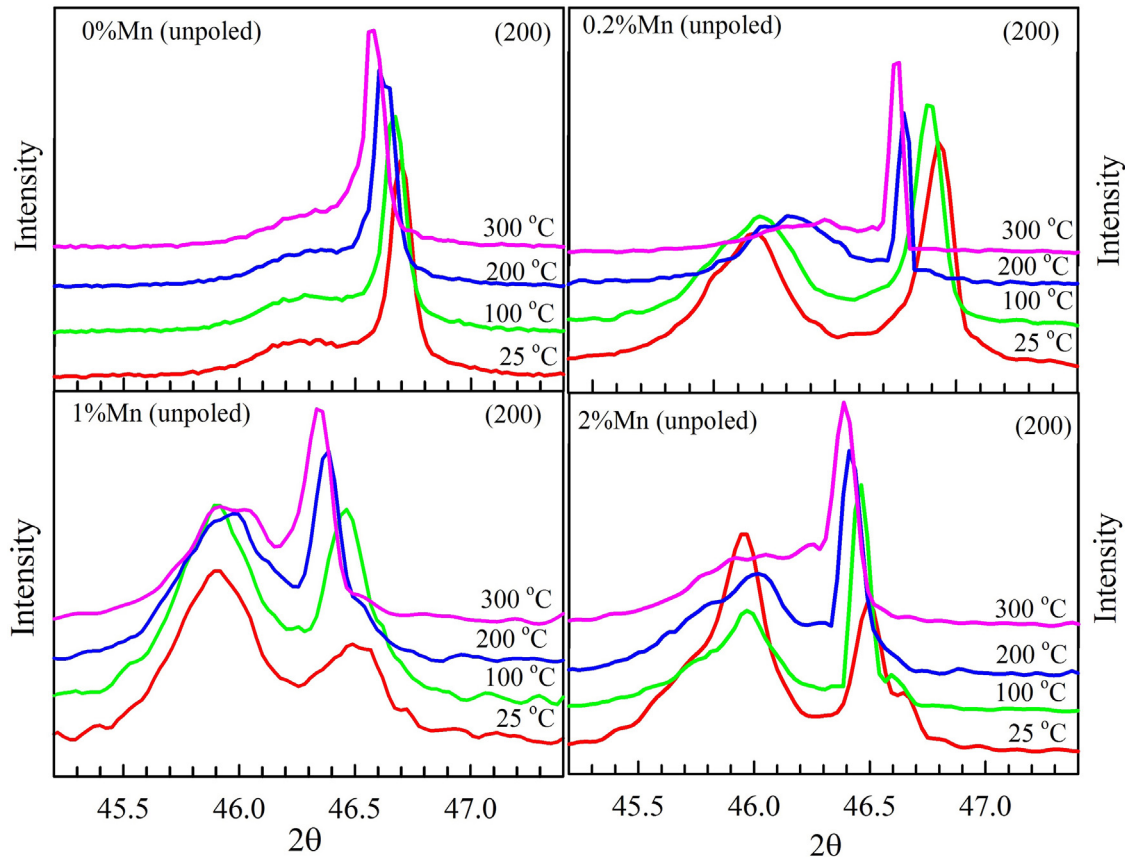


Fig. 9. Synchrotron XRD spectra of (200) Bragg's reflections from 25 to 300 °C.

phase as indicated by green arrow in the inset of Fig. 4(b). The subscript “ortho” signifies the orthorhombic phase. In brief, E(3) mode is characteristic vibration of low-temperature rhombohedral phase [35–38], ν_{ortho} mode is of orthorhombic phase [39,40], and E(1), E(2), $A_1(1)$, B_1 , $A_1(2)$, E(4), and $A_1(3)$ modes are of tetragonal $P4mm$ phase [34,36].

Fig. 5 shows the temperature-dependent Raman spectra from 25 to 290 °C for 0, 0.2, 1, and 2% Mn-doped BN7.5BT. All bands are relatively broad, indicating band overlapping, which is typical feature for perovskite relaxor ferroelectric materials. As shown in Fig. 6(a–d) for 0 and 0.2% Mn, the spectra in the range of 50–700 cm^{-1} were deconvoluted into $A_1(1)$, $A_2(2)$, B_1 , E(5), $A_1(4)$, and E(6) modes at 25 °C and 290 °C. Fig. 6(a) shows the deconvoluted spectrum of 0% Mn at 25 °C. Compared with the pure BNT as given in Tables 1 and 2, the $A_1(1)$ mode exhibits an obvious shift (from 130 to 102 cm^{-1}) and its broad width reveals an increase in the effective mass of the cations and the degree of disorder, respectively. Note that the atomic mass of barium ($m_{\text{Ba}} = 137.34$ amu) lies between the atomic mass of sodium ($m_{\text{Na}} = 22.99$ amu) and bismuth ($m_{\text{Bi}} = 208.98$ amu). Major difference is that $A_1(2)$ mode is accompanied by another mode at 310 cm^{-1} . This mode is identified as B_1 , which is characteristic vibration in the tetragonal phase [28,34,40]. This gives an evidence for two phase coexistence in 0% Mn-doped BN7.5BT. Fig. 6(e–h) shows the spectra for 1 and 2% Mn deconvoluted into 5 dominant modes at 25 and 290 °C. The identified modes are labeled as $\nu_{\text{ortho-1-5}}$. The frequencies of Raman modes at 25 °C

for different compositions are given in Table 2. The frequencies of A-O modes ($A_1(1)$ and $\nu_{\text{ortho-1}}$) for all Mn-doped compositions remains almost the same. The decrease in other vibration frequencies is caused by increase in the effective atomic mass of the B-site cations. This indirectly confirms that the Mn ions occupy B-site of the perovskite unit cell.

Fig. 7 shows the frequency shifts of several noticeable Raman modes as a function of temperature. As shown in Fig. 7(a) for 0% Mn, all frequency modes of $A_1(2)$, B_1 , $A_1(4)$, and E(6) exhibit softening behavior with a minimum near 190 °C. The discontinuous change in vibration frequency indicates a phase transition in ferroelectrics [23,24,41], suggesting that 0% Mn undergoes a structural phase transition near 190 °C. It is consistent with our previous work that 0% Mn undergoes a phase transition from coexistence of rhombohedral $R3c$ and tetragonal $P4bm$ (R+T) phases to tetragonal phase near 200 °C [5].

Fig. 7(b–d) shows temperature dependency of Raman frequencies for 0.2, 1, and 2% Mn. All modes show only slow softening possibly due to freezing-in of Ti/Mn–O vibrations. The frequency variations (from 25 to 290 °C) of dominant B–O vibration modes ($A_1(2)$ and $\nu_{\text{ortho-2}}$) are respectively, 25.3, 24.3, and 18.7 cm^{-1} for 0.2% Mn, 1% Mn, and 2% Mn, implying that the softening behavior decreases as Mn increases. This behavior suggests that Mn doping stabilizes the existing structure. Fig. 8(a–d) shows the temperature-dependent full-width at half maxima (FWHM) of various Raman modes. B–O vibration modes ($A_1(2)$, B_1 , $\nu_{\text{ortho-2}}$ and $\nu_{\text{ortho-3}}$) are weakly affected by

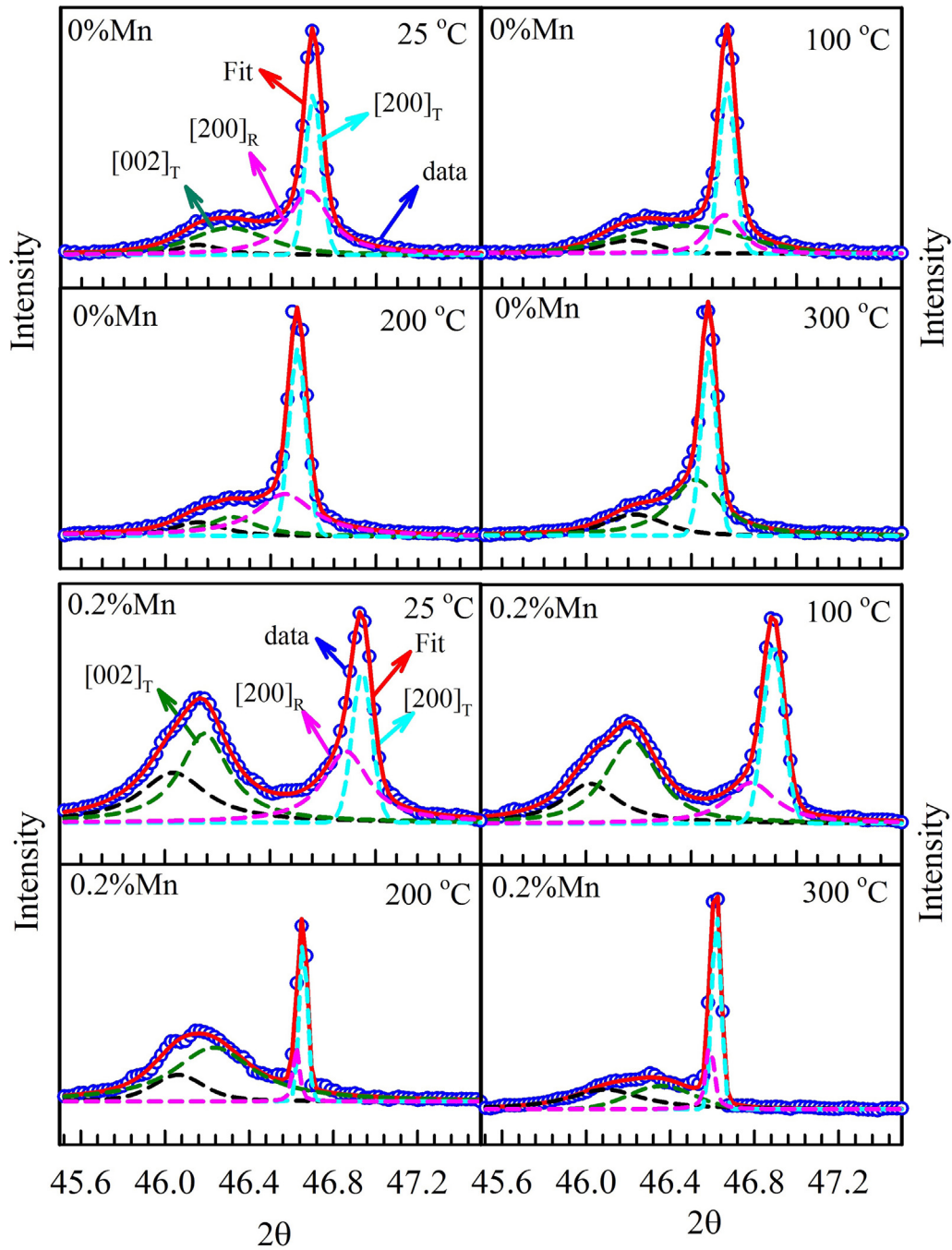


Fig. 10. (200) peaks with fits (Gauss + Lorenz profiles) at 25, 100, 200, and 300 °C for 0 and 0.2% Mn.

temperature. The high-frequency modes ($A_1(4)$, $E(6)$, $\nu_{\text{ortho-4}}$, and $\nu_{\text{ortho-5}}$) of BO_6 octahedra show significant temperature dependence as Mn increases, possibly associated with thermal anharmonicity due to random occupation of Mn ions in the B-site of unit cell.

Synchrotron XRD analysis was carried out in order to correlate it with Raman spectra. Fig. 9 shows the temperature evolution of (200) Bragg's reflections. The peaks become sharper and move to the lower 2θ position, signifying increasing symmetry. In order to understand the phase transitions, diffraction peaks were fitted using Gaussian+Lorentzian profile as

shown in Figs. 10 and 11. The circles in blue represent the experimental data and red solid lines are sums of the fits. At room temperature, the (200) reflection contains $[002]_T$, $[200]_R$, and $[200]_T$ peaks for 0 and 0.2% Mn. The subscripts R and T represent rhombohedral and tetragonal structures. As temperature increases, the (200) reflections become sharp and symmetric. In 0% Mn, the $[200]_R$ peak vanishes above 200 °C and only two tetragonal peaks persist. This suggests that 0% Mn undergoes a structural phase transition from coexistence to tetragonal phase near 200 °C. Similarly, in 0.2% Mn the $[200]_R$ peak persists up to 300 °C as shown in Fig. 10.

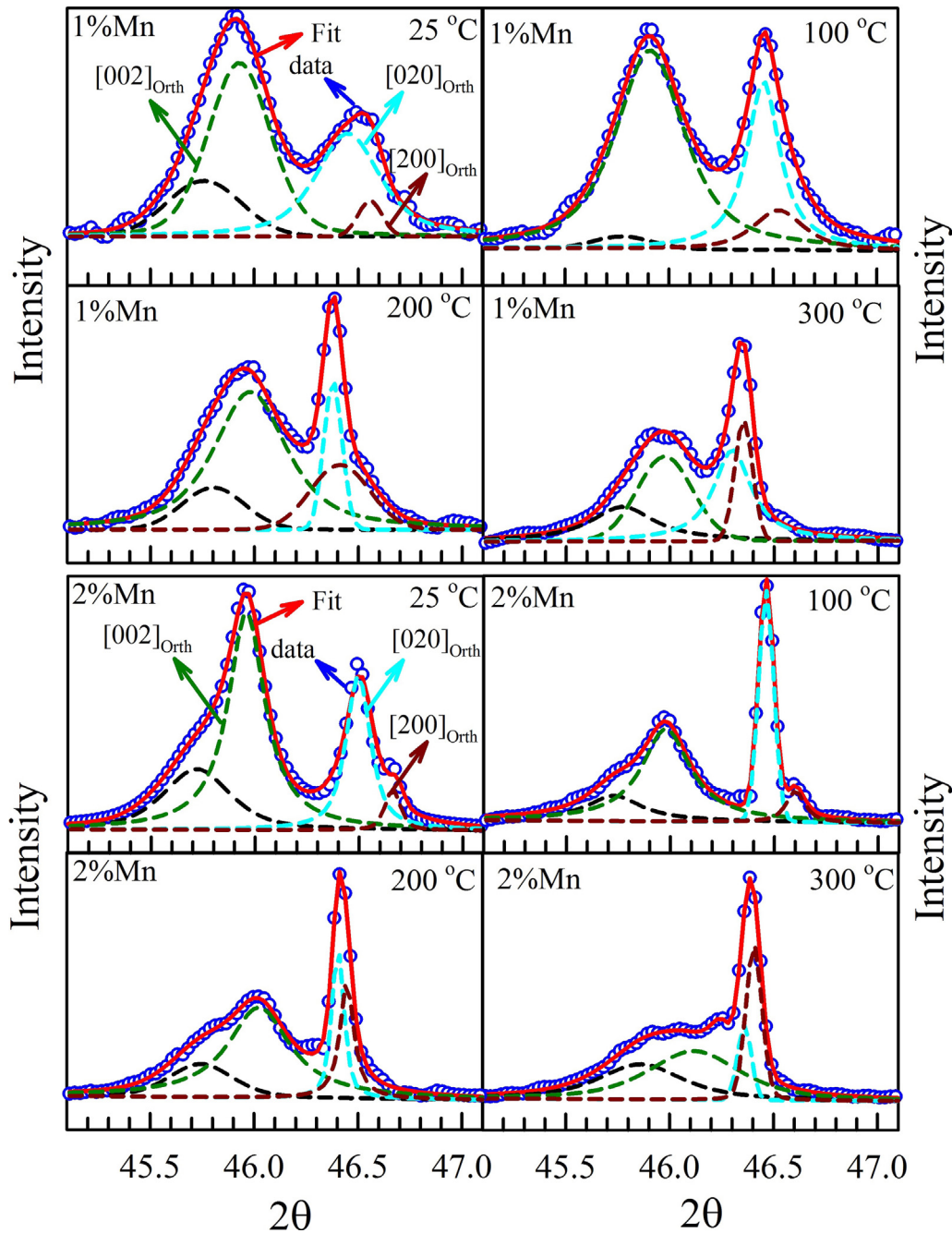


Fig. 11. (200) peaks with fits (Gauss + Lorenz profiles) at 25, 100, 200, and 300 °C for 1 and 2%Mn.

All the XRD reflections have additional peaks, which are marked with black dashed lines. These extra peaks appear at lower 2θ , indicating a coherent superimposition of diffracted waves from nanostructures [42,43]. It is known that the existence of polar nanoregions (PNRs) is a common phenomenon in relaxor systems. These are not only polarized regions, but also displaced along the direction of polarization from their surrounding lattices. When the PNRs sizes are significantly smaller than the coherence length of diffraction radiation, scattered waves from individual nanoregions coherently superimpose to form Bragg reflection peaks, where constructive and destructive interferences lead to significant change in the peak profiles

[43]. These reflections could also be possible from the surface layer, which are often expected in relaxor ferroelectrics to accommodate the lattice distortion [44,45]. Neutron diffraction experiments [44] showed the existence of near-surface regions in the relaxors, and these regions exhibit larger strain than inside the bulk, which is an indicative of substantial distortion in the lattice. The presence of larger strain in the surface layer, contribute significantly to the total diffraction profiles. In 1% and 2% Mn, the room temperature orthorhombic phase persists up to 300 °C, indicated by the presence of $[002]_{\text{Orth}}$, $[020]_{\text{Orth}}$, and $[200]_{\text{Orth}}$ peaks as shown in Fig. 11. These results are consistent with Raman spectra which showed structural phase transition around

190 °C for 0% Mn and only gradual softening behavior up to 290 °C for 0.2, 1, and 2% Mn, as shown in Fig. 7(a–d). These results suggest that the Mn doping stabilizes the structure due to hard character induced by Mn ions [8,9].

4. Conclusions

We have studied the effects of Mn doping in BN7.5BT relaxor ferroelectric ceramics. XAS study reveals an effective equilibrium of divalent Mn^{2+} and trivalent Mn^{3+} in the sintered samples. High-resolution synchrotron XRD and TEM show two-phase coexistence of rhombohedral $R3c$ and tetragonal $P4bm$ structures in 0 and 0.2% Mn-doped BN7.5BT and an orthorhombic (O) structure in 1 and 2% Mn-doped BN7.5BT at room temperature. The 0% Mn-doped BN7.5BT shows a structural transition phase from coexistence (R + T) to T phase near 190 °C, accompanied with a softening anomaly in Raman spectra. Similarly, 0.2–2% Mn-doped BN7.5BT show softening near 290 °C upon heating. This study suggests that Mn ions can enhance structural thermal stability toward higher temperature as revealed by softening behavior of Raman modes.

Acknowledgements

This project is supported by Ministry of Science and Technology of Taiwan, under project Nos. 103-2112-M-030-001, 103-2221-E-146-001, and 102-2221-E-131-006. The advanced Light source is supported by the Director, Office of Science, Office of Basic Energy Sciences, of the U.S. Department of Energy under Contract No. DE-AC02-05CH11231.

References

- [1] Shvartsman VV, Lupascu DC. Lead-free relaxor ferroelectrics. *J Am Ceram Soc* 2012;95(1):1–26.
- [2] Takenaka T, Maruyama K, Sakata K. $(Bi_{1/2}Na_{1/2})TiO_3$ – $BaTiO_3$ system for lead-free piezoelectric ceramics. *Jpn J Appl Phys* 1991;30:2236–9.
- [3] Jo W, Daniels JE, Jones JL, Tan X, Thomas PA, Damjanovic D, et al. Evolving morphotropic phase boundary in lead-free $(Bi_{1/2}Na_{1/2})TiO_3$ – $BaTiO_3$ piezoceramics. *J Appl Phys* 2011;109:014110–14117.
- [4] Anthoniappen J, Lin C-H, Tu CS, Chen P-Y, Chen C-S, Chiu S-J, Lee H-Y, et al. Enhanced piezoelectric and dielectric responses in 92.5% $(Bi_{0.5}Na_{0.5})TiO_3$ –7.5% $BaTiO_3$ ceramics. *J Am Ceram Soc* 2014;97(6):1890–4.
- [5] Anthoniappen J, Tu CS, Chen P-Y, Chen C-S, Chiu S-J, Lee H-Y, et al. Structural phase stability and electric field induced relaxor–ferroelectric phase transition in $(1-x)(Bi_{0.5}Na_{0.5})TiO_3$ – $xBaTiO_3$ ceramics. *J Alloy Compd* 2015;618:120–6.
- [6] Rödel J, Jo W, Seifert KTP, Anton E-M, Granzow T. Perspective on the development of lead-free piezoceramics. *J Am Ceram Soc* 2009;92(6):1153–77.
- [7] Zhou T-S, Huang R-X, Shang X-ZFP, Guo J-Y, Chai L-Y, Gu H-S. Lead-free In_2O_3 -doped $(Bi_{0.5}Na_{0.5})_{0.93}Ba_{0.07}TiO_3$ ceramics synthesized by direct reaction sintering. *Appl Phys Lett* 2007;90:182903–13.
- [8] Priya S, Uchino K. Dielectric and piezoelectric properties of the Mn-substituted $Pb(Zn_{1/3}Nb_{2/3})O_3$ – $PbTiO_3$ single crystal. *J Appl Phys* 2002;91:4515–20.
- [9] Zhang S, Lebrun L, Randall CA, Shrout TR. Growth and electrical properties of (MnF) co-doped $0.92Pb(Zn_{1/3}Nb_{2/3})O_3$ – $0.08PbTiO_3$ single crystal. *J Cryst Growth* 2004;267:204–12.
- [10] Luo L, Zhou D, Tang Y, Jia Y, Xu H, Luo H. Effects of Mn doping on dielectric and piezoelectric properties of $0.71Pb(Mg_{1/3}Nb_{2/3})O_3$ – $0.29PbTiO_3$ single crystals. *Appl Phys Lett* 2007;90:102907–13.
- [11] Yan Y, Cho K-H, Priya S. Identification and effect of secondary phase in MnO_2 -doped $0.8Pb(Zr_{0.52}Ti_{0.48})O_3$ – $0.2Pb(Zn_{1/3}Nb_{2/3})O_3$ piezoelectric ceramics. *J Am Ceram Soc* 2011;94(11):3953–9.
- [12] Priya S, Uchino K, Ryu J, Ahn CW, Nahm S. Induction of combinatory characteristics by relaxor modification of $Pb(Zr_{0.5}Ti_{0.5})O_3$. *Appl Phys Lett* 2003;83(24):5020–2.
- [13] Zhang Q, Zhang Y, Wang F, Wang Y, Lin D, Zhao X, et al. Enhanced piezoelectric and ferroelectric properties in Mn-doped $Na_{0.5}Bi_{0.5}TiO_3$ – $BaTiO_3$ single crystals. *Appl Phys Lett* 2009;95:102904–13.
- [14] Sapper E, Schaab S, Jo W, Granzow T, Rödel J. Influence of electric fields on the depolarization temperature of Mn-doped $(1-x)(Bi_{0.5}Na_{0.5})TiO_3$ – $xBaTiO_3$. *J Appl Phys* 2012;111:014105–14106.
- [15] Zhu M, Liu L, Hou Y, Wang H, Yan H. Microstructure and electrical properties of MnO-doped $(Na_{0.5}Bi_{0.5})_{0.92}Ba_{0.08}TiO_3$ lead-free piezoceramics. *J Am Ceram Soc* 2007;90(1):120–4.
- [16] Yao J, Yang Y, Monsegue N, Li Y, Li J, Zhang Q, et al. Effect of Mn substituents on the domain and local structures of $(Na_{1/2}Bi_{1/2})TiO_3$ – $BaTiO_3$ single crystals near a morphotropic phase boundary. *Appl Phys Lett* 2011;98:132903–13.
- [17] Guennou M, Savinov M, Drahoukoupil J, Luo H, Hlinka J. High piezoelectric coefficient of single domain Mn-doped NBT-6%BT single crystals. *Appl Phys A* 2014;116:225–8.
- [18] Wang S-F, Tu C-S, Chang T-L, Chen P-Y, Chen C-S, Schmidt VH, Anthoniappen J. Structural stability and depolarization of manganese-doped $(Bi_{0.5}Na_{0.5})_{1-x}Ba_xTiO_3$ relaxor ferroelectrics. *J Appl Phys* 2014;116:154101–9.
- [19] Rousseau DL, Bauman RP, Porto SPS. Normal mode determination in crystals. *J Raman Spectroscopy* 1981;10(1):253–90.
- [20] Pezzotti G. Raman spectroscopy of piezoelectrics. *J Appl Phys* 2013;113:21130–78.
- [21] Jones GO, Thomas PA. Investigation of the structure and phase transitions in the novel A-site substituted distorted perovskite compound $Na_{0.5}Bi_{0.5}TiO_3$. *Act Crystallogr B* 2002;B58:168–78.
- [22] Petzelt J, Kamba S, Fabbry J, Noujni D, Porokhonskyy V, Pashkin A, et al. Infrared, Raman and high-frequency dielectric spectroscopy and the phase transitions in $Na_{1/2}Bi_{1/2}TiO_3$. *J Phys: Condens Matter* 2004;16(15):2719–31.
- [23] Barick BK, Mishra KK, Arora AK, Choudhary RNP, Pradhan DK. Impedance and Raman spectroscopic studies of $(Na_{0.5}Bi_{0.5})TiO_3$. *J Phys D: Appl Phys* 2011;44:355402 (10pp).
- [24] Kreisel J, Glazer AM, Jones G, Thomas PA, Abello L, Lucazeau G. An X-ray diffraction and Raman spectroscopy investigation of A-site substituted perovskite compounds: the $(Na_{1-x}K_x)_{0.5}Bi_{0.5}TiO_3$ ($0 \leq x \leq 1$) solid solution. *J Phys: Condens Matter* 2000;12:3267–80.
- [25] Jones GO, Thomas PA. The tetragonal phase of $Na_{0.5}Bi_{0.5}TiO_3$ —a new variant of the perovskite structure. *Acta Crystallogr B* 2000;B56:426–30.
- [26] Kreisel J, Glazer AM. High-pressure Raman study of a relaxor ferroelectric: the $Na_{0.5}Bi_{0.5}TiO_3$ perovskite. *Phys Rev B: Condens Matter* 2001;63:174106–10.
- [27] Tripathy SN, Mishra KK, Sen S, Pradhan DK. Dielectric and Raman spectroscopic studies of $Na_{0.5}Bi_{0.5}TiO_3$ – $BaSnO_3$ ferroelectric system. *J Am Ceram Soc* 2014;97(6):1846–54.
- [28] Suchanicz J, Sumara IJ, Kruzina TV. Raman and infrared spectroscopy of $Na_{0.5}Bi_{0.5}TiO_3$ – $BaTiO_3$ ceramics. *J Electroceram* 2011;27:45–50.
- [29] Zhang M-S, Scott JF, Zvirgzds JA. Raman spectroscopy of $Na_{0.5}Bi_{0.5}TiO_3$. *Ferroelectr Lett Sect* 1986;6(5):147–52.
- [30] Luo L, Ge W, Li J, Viehland D, Farley C, Bodnar R, et al. Raman spectroscopic study of $Na_{1/2}Bi_{1/2}TiO_3$ – $x%BaTiO_3$ single crystals as a function of temperature and composition. *J Appl Phys* 2011;109:113507–16.
- [31] Tarte P, Rulmont A, Liégeois-Duyckaerts M, Cahay R, Winand JM. Vibrational spectroscopy and solid state chemistry. *Solid State Ionics* 1990;42:177–96.
- [32] Sendova M, Hosterman BD, Raud R, Hartmann T, Koury D. Temperature-dependent, micro-Raman spectroscopic study of barium titanate nanoparticles. *J Raman Spectrosc* 2015;46:25–31.

- [33] Buscaglia V, Buscaglia MT, Viviani M, Ostapchuk T, Gregora I, Petzelt J, et al. Raman and AFM piezoresponse study of dense BaTiO₃ nanocrystalline ceramics. *J Eur Ceram Soc* 2005;25:3059–62.
- [34] Venkateswaran UD. High-pressure Raman studies of polycrystalline BaTiO₃. *Phys Rev B: Condens Matter* 1998;58:14256–60.
- [35] Mejia-Uriarte EV, Sato-Berrú RY, Navarrete M, Kolokoltsev O, Saniger JM. Determination of phase transition by principal component analysis applied to Raman spectra of polycrystalline BaTiO₃ at low and high temperatures. *J Appl Res Technol* 2012;10:57–62.
- [36] Perry CH, Hall DB. Temperature dependence of the Raman spectrum of BaTiO₃. *Phys Rev Lett* 1965;15:700–2.
- [37] Upendra AJ, Songhak Y, Sungg B, Jae SL. Surfactant-free hydrothermal synthesis of highly tetragonal barium titanate nanowires: a structural investigation. *J Phys Chem B* 2006;110:12249–56.
- [38] Frey MH, Payne DA. Grain-size effect on structure and phase transformations for barium titanate. *Phys Rev B: Condens Matter* 1996;54:3158–68.
- [39] Shiratori Y, Pithan C, Dornseiffer J, Waser R. Raman scattering of studies on nanocrystalline BaTiO₃ Part I—isolated particles and aggregates. *J Raman Spectrosc* 2007;38:1288–99.
- [40] Domenico Jr MD, Wemple SH, Porto SPS. Raman spectrum of single-domain BaTiO₃. *Phys Rev* 1968;174:522–30.
- [41] Cheng J, Yang Y, Tong Y-H, Lu S-B, Sun J-Y, Zhu K, et al. Study of monoclinic-tetragonal-cubic phase transition in Pb(Zn_{1/3}Nb_{2/3})O₃–0.08PbTiO₃ single crystals by micro-Raman spectroscopy. *J Appl Phys* 2009;105:053519.
- [42] Chang WS, Lim LC, Yang P, Miao H, Tu CS, Chen Q, et al. Tetragonal micro/nanotwins in 0.91Pb(Zn_{1/3}Nb_{2/3})O₃–0.09PbTiO₃ revealed by reciprocal space mapping. *Appl Phys Lett* 2009;94:202907–13.
- [43] Wang YU. Diffraction theory of nanotwin superlattices with low symmetry phase: application to rhombohedral nanotwins and monoclinic MA and MB phases. *Phys Rev B: Condens Matter* 2007;76:024108–24111.
- [44] Conlon KH, Luo H, Viehland D, Li JF, Whan T, Fox JH, et al. Direct observation of the near-surface layer in Pb(Mg_{1/3}Nb_{2/3})O₃ using neutron diffraction. *Phys Rev B: Condens Matter* 2004;70:172204–14.
- [45] Xu G, Hiraka H, Shirane G. Dual structures in (1–x)Pb(Zn_{1/3}Nb_{2/3})O₃–xPbTiO₃ ferroelectric relaxors. *Appl Phys Lett* 2004;84:3975–7.